

Corrosion behavior of zinc-nickel and graphene layered structures on steel substrates

Georgios Polizos¹, Yijing Y. Stehle¹, Jaswinder Sharma¹, Dmitry Voylov², Ivan Vlassiouk¹, Seungha Shin³, Harry M. Meyer III⁴

¹Energy and Transportation Science Division, Oak Ridge National Laboratory, Oak Ridge, TN 37831, USA

²Department of Chemistry, University of Tennessee, Knoxville, TN 37996, USA

³Department of Mechanical, Aerospace and Biomedical Engineering, University of Tennessee, Knoxville, TN 37996, USA

⁴Materials Science and Technology Division, Oak Ridge National Laboratory, Oak Ridge, TN 37831, USA

Keywords: Graphene, zinc-nickel, corrosion, salt fog

NOTICE OF COPYRIGHT

This manuscript has been authored by UT-Battelle, LLC under Contract No. DE-AC05-00OR22725 with the U.S. Department of Energy. The United States Government retains and the publisher, by accepting the article for publication, acknowledges that the United States Government retains a non-exclusive, paid-up, irrevocable, worldwide license to publish or reproduce the published form of this manuscript, or allow others to do so, for United States Government purposes. The Department of Energy will provide public access to these results of federally sponsored research in accordance with the DOE Public Access Plan (<http://energy.gov/downloads/doe-public-access-plan>).

Abstract

Large-area single layers of graphene were synthesized using chemical vapor deposition techniques and were assembled onto steel substrates that were finished with a thin layer of electrodeposited zinc-nickel (ZnNi). Atomic force microscopy combined with Raman spectroscopy was used to determine the number of the assembled graphene layers and to characterize the defects in their crystal structure. The graphene-ZnNi-steel layered specimens were exposed to a salt-fog environment. The defects in the structure of the graphene single layers were found to accelerate corrosion and the formation of a resistive oxide layer. The chemical composition and element map of the reacted surfaces were studied by x-ray photoelectron spectroscopy. The electrical properties of the samples before and after the salt-fog testing were evaluated using sheet resistance measurements.

1. Introduction

Corrosion and associated maintenance costs are major concerns when metallic surfaces are exposed to environmental conditions.^[1-4] For example, electrically conductive components of power systems and electrical equipment are vulnerable to corrosion, and the buildup of oxide layers increases electrical resistance and can cause electrical failures. Coatings based on hexavalent chromium and cadmium can provide sufficient corrosion resistance while maintaining low electrical resistance. However, their use is limited due to the health and environmental concerns related to waste generation and to the hazardous nature of those materials. Coatings based on zinc-nickel (ZnNi) are commonly being used to protect electrical components from corrosion. Although their corrosion resistance needs to be improved, they are considered a substitute for the hexavalent chromium and cadmium coatings.

Graphene is a conductive two-dimensional (2D) material with excellent barrier properties and chemical resistance.^[5] It has a wide range of potential applications as an ultrathin conductor in electrical and electronic components. The anticorrosion properties of the graphene are of significant technological importance. Coatings based on graphene have shown promising anti-corrosion properties.^[6-9] However, the formation of defects and cracks in the structure of the coatings can accelerate corrosion because graphene is cathodic to several metals.^[10,11]

Graphene coatings produced by chemical vapor deposition (CVD) have several advantages over graphene paints, which are based on aggregates of exfoliated graphene nanoplatelets. CVD is a facile method that can be scaled to synthesize high-quality, large-scale single layers of graphene.^[12] We report our studies on the corrosion mechanism of graphene-based coatings that we assembled by applying onto a conductive substrate single-layer graphene sheets that we synthesized by CVD techniques. The synthesized graphene sheets were assembled on top of steel substrates that were finished with an 8 μm thick layer of electrodeposited ZnNi. The structures were subjected to salt-fog testing. The formation and electrical properties of the resistive reacted layer were investigated.

2. Experimental

Large-area single-layer graphene sheets were synthesized using CVD techniques. The CVD setup and synthesis procedure as well as a description of the x-ray photoelectron spectroscopy (XPS) and scanning electron microscopy (SEM) setup are provided elsewhere.^[13-15] Wide-energy-range XPS survey scans and narrow-energy-range core level spectra were acquired to determine and analyze the elements on the surface of the samples. The surface composition was also measured after approximately 280 nm of surface material was removed by etching with Ar ions (the Ar ion energy was 2 kV). The distribution of C, O, Cl, and

Zn was measured in an area approximately 3×4 mm in the mid-region of each sample. An array of 130 (10×13) analysis points was defined in the center of each sample, and the C 1s, O 1s, Cl 2p, and Zn 2p_{3/2} core level spectra were acquired at each point. Element maps were obtained before and after the salt-fog testing. A Horiba atomic force microscope (AFM) equipped with a Raman spectrometer (AFM-Raman) was used for the surface characterization of the assembled graphene sheets. Steel substrates (1018 grade) were custom-ordered with and an 8 μ m thick coating of ZnNi according to ASTM B-841. Three single-layers of graphene were transferred and assembled onto the ZnNi-steel substrates. Salt-fog experiments were performed according to the ASTM B-117 protocol. A Jandel four-point probe was used to measure the sheet resistance of the coatings. The sample designation is as follows: ZnNi-steel with three single layers of graphene (ZnNi-Graphene); ZnNi-steel without graphene (ZnNi).

3. Results and discussion

Single layers of graphene were grown on a copper foil catalyst. Poly(methyl methacrylate) (PMMA) was used to spin-coat the graphene layers and transfer them onto the ZnNi substrates after the copper was dissolved. The samples were rinsed with acetone and were annealed to remove the PMMA.^[14] The process was repeated to assemble three single layers of graphene onto three 1×1 in. ZnNi substrates. SEM images of the ZnNi surface prior to the assembly of the graphene layers are shown in Figures 1a and b. After the annealing and thermal degradation process the PMMA was not entirely removed from the surface of the assembled graphene layers.

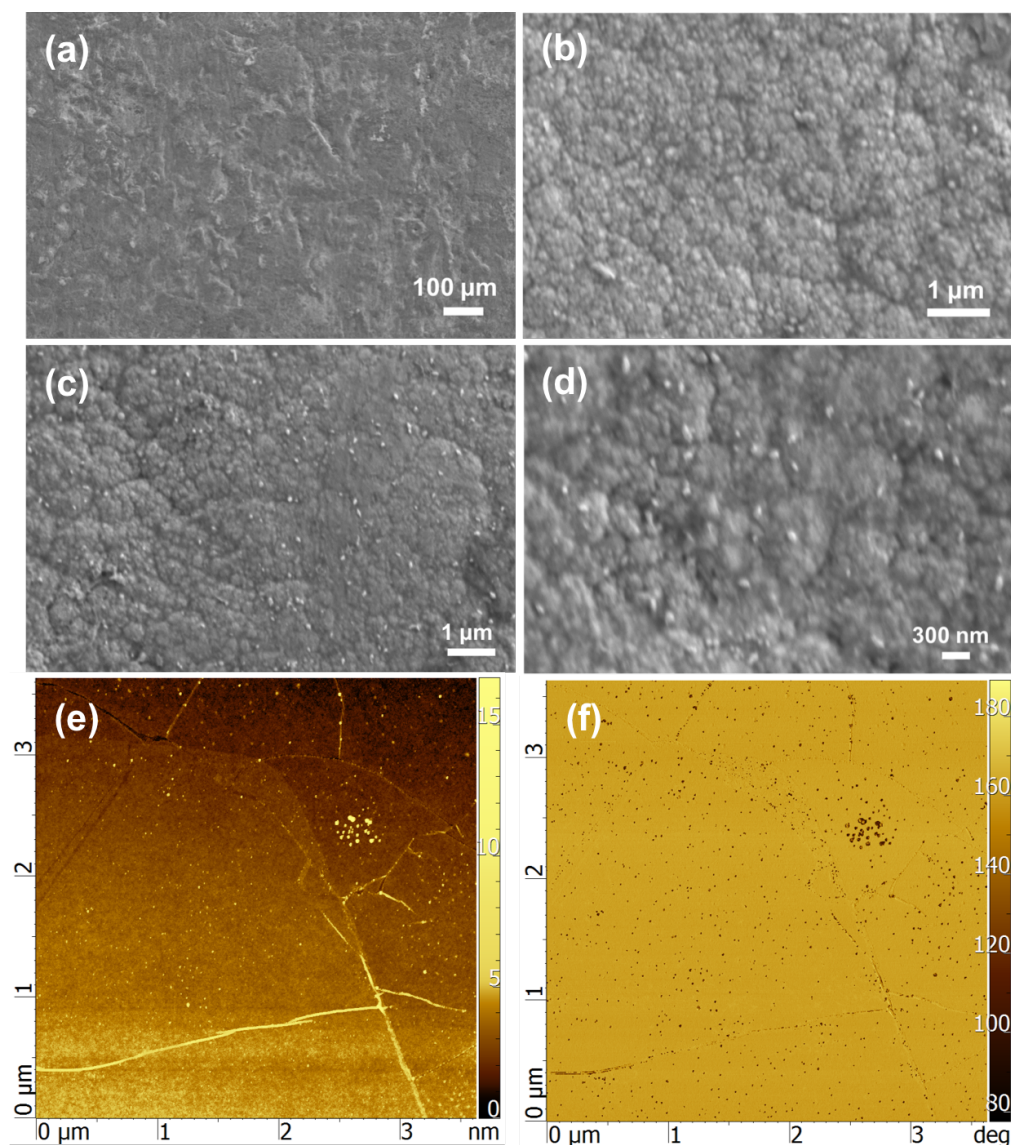


Figure 1. (a,b) SEM images of the ZnNi substrates. (c,d) SEM images of the assembled graphene layers on the ZnNi substrates. (e,f) AFM topography and phase imaging of the copper foil with graphene and PMMA after annealing.

PMMA residues less than 100 nm in size remained on the surface of the assembled graphene layers (Figures 1c and d). Copper foil with graphene and PMMA was annealed to verify that the particulate clusters on the graphene surface were not associated with surface contamination during the transfer process. The AFM topography and phase imaging of the annealed copper

(Figures 1e and f, respectively) show similar clusters of the same size; those clusters are attributed to PMMA residues that could not be completely removed.^[16–18]

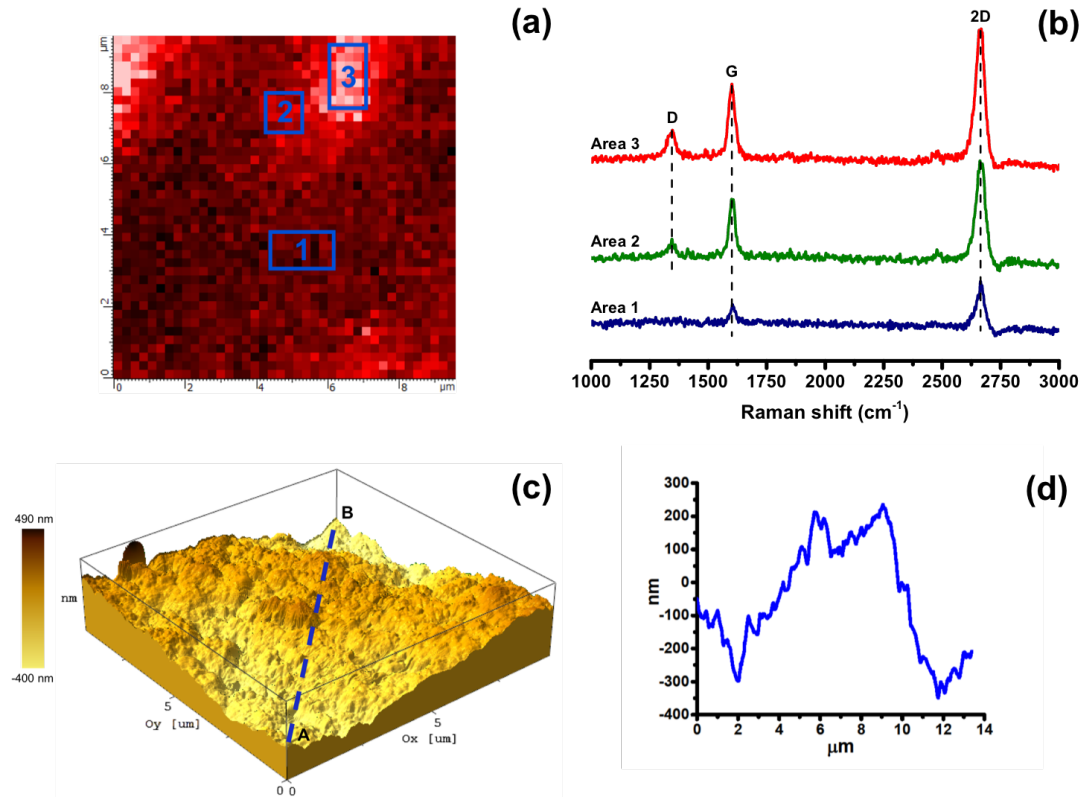


Figure 2. Raman-AFM measurements of large-area single-layer graphene sheets assembled onto the ZnNi layer. (a) Raman map for a single layer of graphene. (b) A comparison plot for the Raman spectra of the three marked areas in the Raman scan. (c) AFM micrograph showing the surface topography of the assembled three graphene layers. (d) Surface profile for the line scan across points A and B in the AFM micrograph.

AFM-Raman measurements were performed on the assembled layers. The Raman scan for a single layer of graphene is shown in Figure 2a. A comparison Raman plot for three areas with markedly different spectra is shown in Figure 2b. The peaks around 1,599 and 2,665 cm^{-1} are closely positioned to the characteristic G and 2D bands for a single layer of graphene.^[19,20] The peak at 1,346 cm^{-1} is associated with the formation of defects and structural disorders in the

graphene crystal.^[21,22] The intensity of that peak was found to vary among the measured areas. Areas where the D band is absent are defect-free (e.g., area 1 in Figure 2a). The formation of the D band (areas 2 and 3 in Figure 2a) is associated with the onset of the defect formation. The intensity ratio of the D and G bands is associated with the characteristic length scales for the defect sizes and the distances between defects.^[21-24] Structural defects are expected to form during the synthesis and transfer of the large-scale graphene single layers. A three-layer graphene configuration was used to provide better protection of the ZnNi-steel substrates against corrosion. The topography of the three assembled graphene layers is shown in the AFM micrograph in Figure 2c. The surface features are pronounced and vary in height by a few hundred nanometers (see Figure 2d, a line scan from point A to point B in Figure 2c). This rather high value is attributed to the surface features of the ZnNi substrate (Figure 1a, b), the PMMA residues on the surface of the graphene, and the formation of surface wrinkles during the transfer and assembly process.

The survey spectra and the measured surface composition of the sample with three single layers of graphene (ZnNi-Graphene) are shown in Figure 3a. Spectra were acquired before and after the surface of the sample was etched with Ar ions. Optical images of the measured areas are also shown in Figure 3a. Carbon and oxygen are the most prevalent elements on the surface of the pristine ZnNi-Graphene sample. The surface of the sample was etched with Ar ions to remove surface contaminants. After etching, the surface concentrations of Zn, Ni, O, and C were 63.3, 32.4, 3.2, and 1.1 at. %, respectively. The depth profile of the coating composition is shown in Figure 3b.

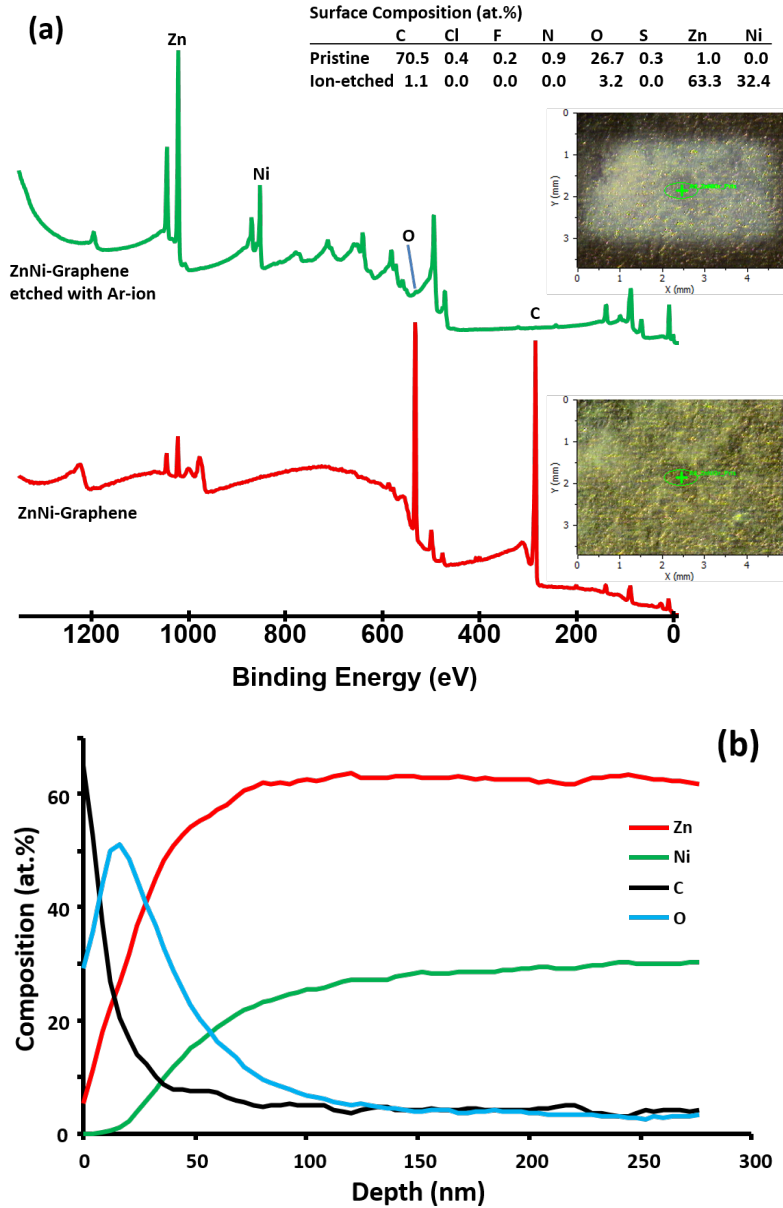


Figure 3. (a) XPS survey spectra and surface composition for the ZnNi-Graphene sample before and after etching with Ar ions. The optical images of the samples are also shown. The green oval with the cross symbol is the approximate size of the x-ray spot on the sample and the measured composition is an average of that area. (b) The depth profile of the coating composition according to the XPS measurements.

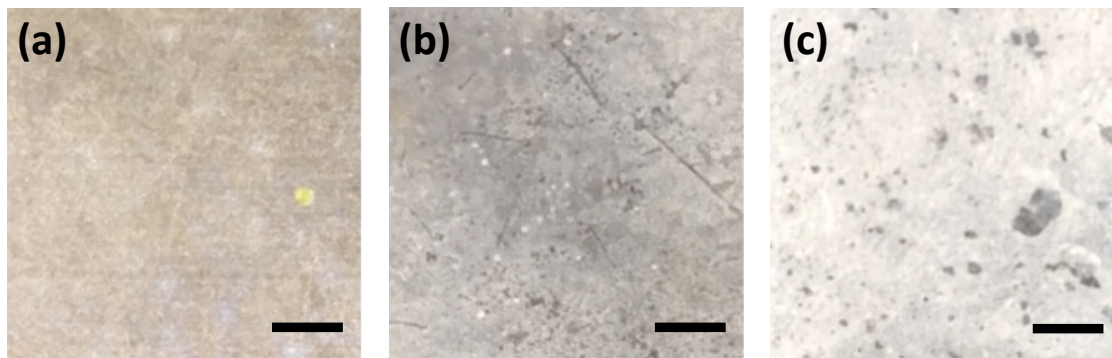


Figure 4. Optical images of the samples before and after 48 h exposure to salt fog. (a) ZnNi-Graphene before testing. (b) ZnNi after the salt-fog test. (c) ZnNi-Graphene after the salt-fog test. The scale bars are 5 mm.

Corrosion testing of the samples was performed in a salt-fog chamber. Optical images of the samples' surfaces are shown in Figure 4. The pristine (prior to testing) ZnNi-Graphene is shown in Figure 4a. The ZnNi-steel without graphene (ZnNi), and the ZnNi-Graphene after 48 h exposure in the salt-fog chamber are shown in Figures 4b and c, respectively. The graphene was found to accelerate the corrosion of the ZnNi layer. The formation of a reacted (corroded) layer was more pronounced for the ZnNi-Graphene sample (Figure 4c) than it was for the ZnNi sample. The chemical compositions of the samples' surfaces was calculated using XPS measurements. The XPS survey spectra for the ZnNi specimen after 48 h of testing are shown in Figure 5. After etching the sample with Ar ions to remove surface contaminants, the predominant elements on the surface are Zn, O, and C, and the respective concentrations are 46.0, 46.6, and 5.1 at.%. Similarly high Zn and O concentrations were calculated for the ZnNi-Graphene sample that was etched with Ar ions after the completion of the salt-fog testing (Zn: 37.2 at.%, O: 46.0 at.%, C: 6.1 at.%; the XPS data are not presented here).

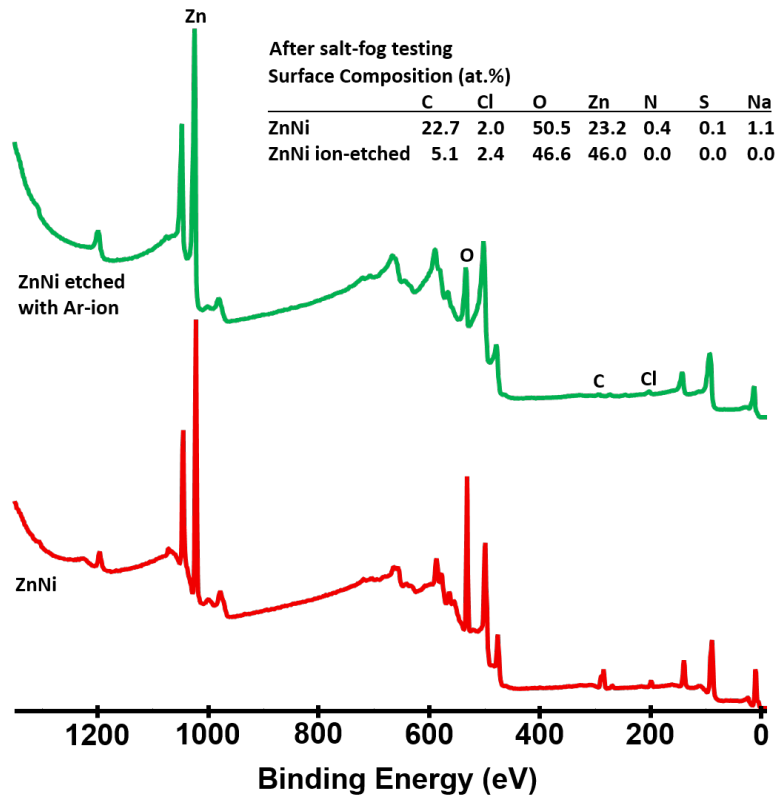


Figure 5. XPS survey spectra and surface composition for the ZnNi sample after 48 h of testing in the salt-fog chamber. Measurements were performed before and after the surface was etched with Ar ions.

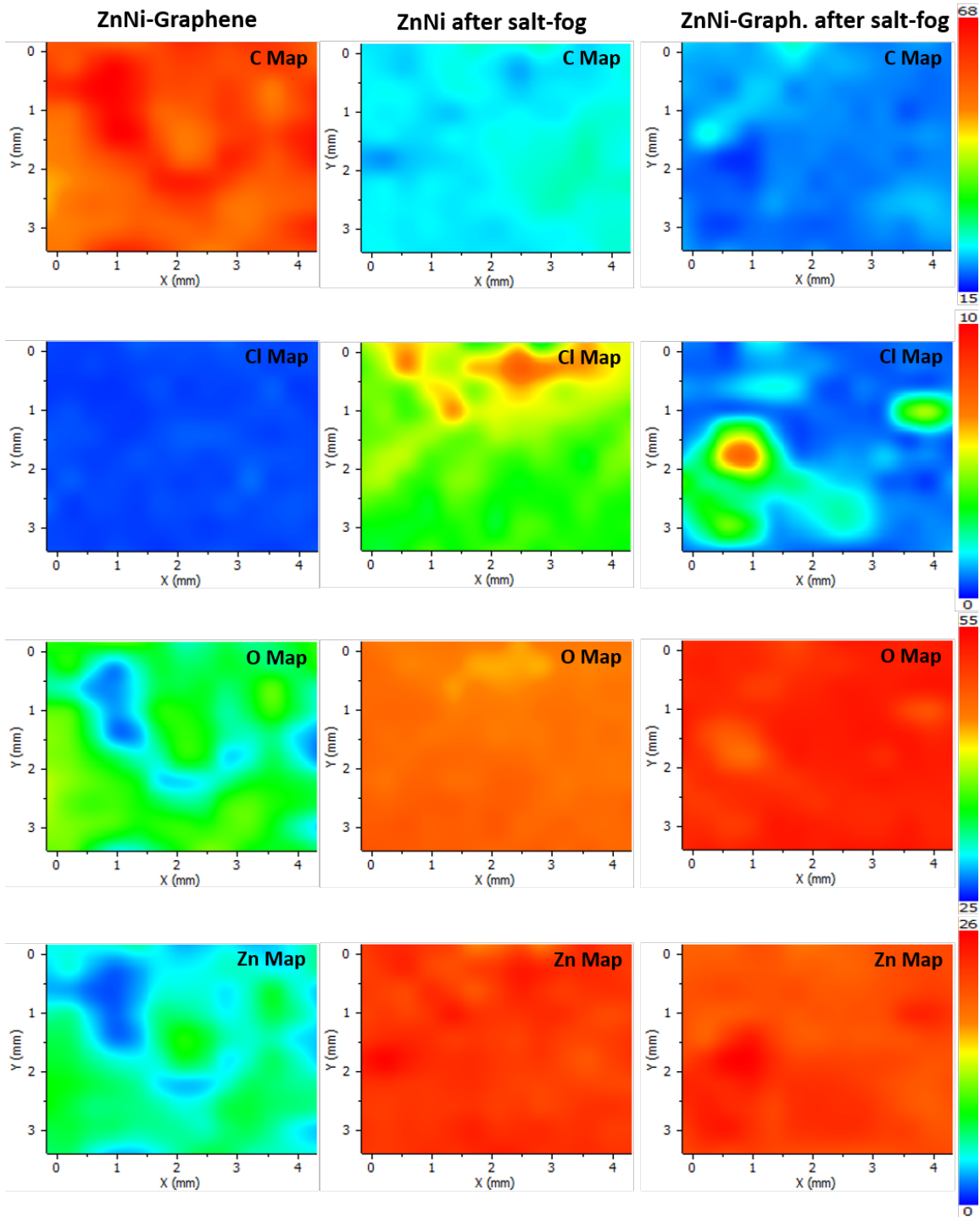


Figure 6. Element maps for the C, O, Zn, and Cl on the surface of the pristine ZnNi-Graphene, ZnNi, and ZnNi-Graphene after the salt-fog testing. The scale bars to the right are atomic percent and were selected to be the same for each of the three samples so that they could be directly compared.

The element maps for the C, O, Zn, and Cl on the surface of the samples are shown in Figure 6. There is an inhomogeneous distribution of the surface composition, with regions of lower and higher C content, lower and higher Zn-O content, and spots of observable Cl. As expected, C is the predominant element in the pristine (prior to the salt-fog testing) ZnNi-Graphene sample. The maps for O and Zn clearly show a correlation between those two elements. After the salt-fog testing, O and Zn are the elements with the highest atomic percentages across the surface, indicating that the reacted surface is primarily ZnO. The small amount of Cl can be attributed to residues that contaminated the surfaces of the samples while transferring the graphene layers onto the ZnNi substrates (FeCl_3 was used to dissolve the Cu foil prior to the graphene transfer). In addition, Cl could have contaminated the surface of the samples during the salt-fog experiments.

A comparison plot for the C 1s spectra is shown in Figure 7. Two peaks are present in all samples. The peak at approximately 285 eV is attributed to surface-adsorbed C species, whereas the peak at approximately 290 eV is attributed to carbonate species, such as zinc-carbonate.^[25] After the samples were etched with Ar ions, the C and carbonate species were removed from the surface of the pristine ZnNi-Graphene sample. For the reacted ZnNi, C that was adsorbed to the surface was mostly removed after the ion etching; however, the carbonate species were still present, which indicates that they were part of the reaction layer. For the reacted ZnNi-Graphene sample, there was still a significant amount of surface C even after the ion-etching, which indicates that the graphene was incorporated into the reacted layer. The peak that is attributed to the carbonate species is more pronounced than the peak attributed to the reacted ZnNi sample, even after the ion etching of the surface. The graphene layers accelerated the corrosion of the ZnNi layer and resulted in the formation of a thicker corroded layer, which is clearly shown in Figure 4c.

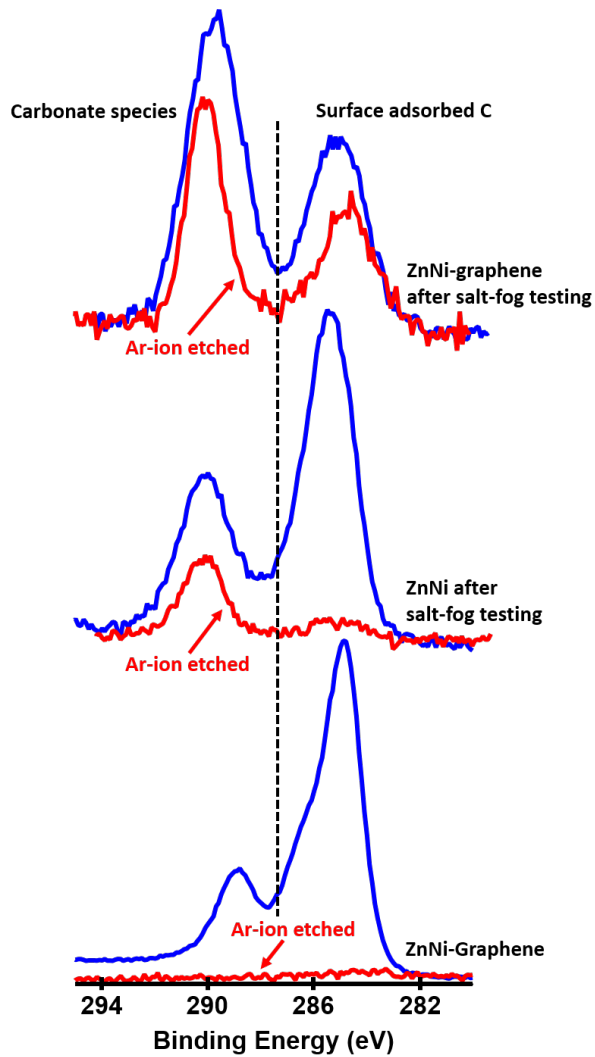


Figure 7. A comparison plot for the C 1s spectra for the pristine ZnNi-Graphene, ZnNi, and ZnNi-Graphene after the salt-fog testing.

The sheet resistance of the reacted layer was measured using a four-point probe. The sheet resistance of the pristine ZnNi and ZnNi-Graphene samples was varied from a few to 100 Ω /sq across the surface. The measured values are similar to the sheet resistance values of single-layer and multilayer graphene configurations reported in the literature. Approximately 30 Ω /sq is the theoretical resistance value for a single layer.^[26,18] The measured sheet resistance values for a

single layer and a few layers of graphene range from 100 to a few hundred Ω/sq .^[27–30,18] After the salt-fog testing, the sheet resistance values were increased significantly. The values of the ZnNi sample were heterogeneous and varied across different areas. The lowest measured values were less than 100 Ω/sq , whereas the sheet resistance values in areas with more evident oxidation were in the $\text{k}\Omega/\text{sq}$ range or even a few $\text{M}\Omega/\text{sq}$. This noticeable variation can be attributed to the heterogeneous growth of the reacted layer due to the inhomogeneous element composition across the surface as well as to variations in the thickness of the reacted layer. The progression of the corrosion for the ZnNi-Graphene sample was more evident. The entire surface was corroded, and the sheet resistance was several hundred $\text{M}\Omega/\text{sq}$ or higher.

A schematic illustration of the corrosion mechanism is shown in Figure 8. Defect sites in the assembled graphene layers can form hydrophilic gates that allow the diffusion of water molecules, oxygen, and salt ions. The defects can induce or accelerate corrosion.^[31–34] The pore size that is required for the water and ion transport is in the sub-nanometer range according to computer simulation studies of desalination membranes.^[35] Oxygen radicals on the graphene surface can also assist the transport of water and ions between the graphene layers; that mechanism is similar to the transport mechanism of hydrated ions in graphene oxide membranes.^[36] Recent studies of polycrystalline graphene-Cu substrates indicate that the grain boundaries can play a significant role in the oxidation of the metal substrate through the inversion of the epoxide groups in the presence of OH and O atoms.^[37]

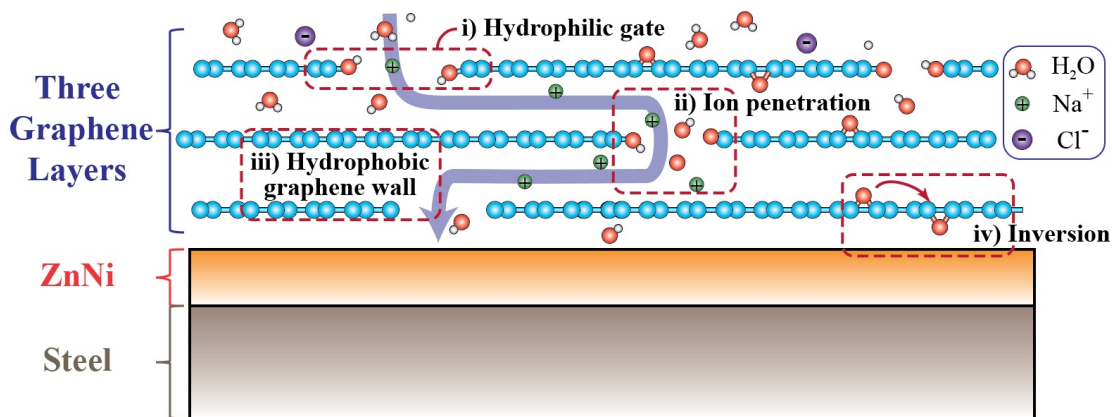


Figure 8. Schematic illustration of the water and ion diffusion through the defects in the structure of the graphene layers.

4. Conclusions

The corrosion resistance of large-area graphene was investigated. Three single layers of graphene were assembled onto steel substrates that were finished with electrodeposited ZnNi. AFM-Raman measurements on the surface of the assembled layers showed the formation of defects and structural disorders in the graphene crystal. Such defects can be formed during the synthesis and transfer of the graphene layers. Graphene-ZnNi-steel specimens and ZnNi-steel substrates were tested in a salt-fog chamber. The corrosion and the formation of a resistive oxide layer was found to be accelerated on the graphene-ZnNi-steel substrates. XPS measurements showed an inhomogeneous distribution of the surface composition, with O and Zn being the elements with the highest atomic percentages.

Notes

The authors declare no competing financial interest.

Acknowledgments

This research was supported by the US Strategic Environmental Research and Development Program (SERDP) under contract WP-2524. GP acknowledges financial support by the US Department of Energy's Office of Vehicle Technologies. DV thanks the US Department of Energy, Office of Science, Basic Energy Sciences, Materials Science & Engineering Division for partial financial support. The authors would like to thank Nathan Wood from Oak Ridge National Laboratory for his help with the salt-fog experiments. Oak Ridge National Laboratory is operated for the US Department of Energy by UT-Battelle under contract no. DE-AC05-00OR22725.

References

- [1] R. E. Ricker, *Science* **1991**, 252, 1232.
- [2] G. H. Koch, M. P. H. Brongers, N. G. Thompson, Y. P. Virmani, J. H. Payer, Corrosion costs and preventive strategies in the United States *Report FHWA-RD-01-156* **2001**.
- [3] K. Vignarooban, X. Xu, A. Arvay, K. Hsu, A. M. Kannan, *Appl. Energy* **2015**, 146, 383.
- [4] S. Thomas, N. V. Medhekar, G. S. Frankel, N. Birbilis, *Curr. Opin. Solid State Mater. Sci.* **2015**, 19, 85.
- [5] Y. Su, V. G. Kravets, S. L. Wong, J. Waters, A. K. Geim, R. R. Nair, *Nat. Commun.* **2014**, 5, 4843.
- [6] M. F. Montemor, *Surf. Coat. Technol.* **2014**, 258, 17.
- [7] M. Mo, W. Zhao, Z. Chen, Q. Yu, Z. Zeng, X. Wu, Q. Xue, *RSC Adv.* **2015**, 5, 56486.
- [8] M. J. Nine, M. A. Cole, L. Johnson, D. N. H. Tran, D. Losic, *ACS Appl. Mater. Interfaces* **2015**, 7, 28482.

- [9] J. H. Huh, S. H. Kim, J. H. Chu, S. Y. Kim, J. H. Kim, S. Y. Kwon, *Nanoscale* **2014**, 6, 4379.
- [10] M. Schriver, W. Regan, W. J. Gannett, A. M. Zaniwski, M. F. Crommie, A. Zettl, *ACS Nano* **2013**, 7, 5763.
- [11] C. Cui, A. T. O. Lim, J. Huang, *Nat. Nanotechnol.* **2017**, 12, 834.
- [12] I. V. Vlassiouk, Y. Stehle, P. R. Pudasaini, R. R. Unocic, P. D. Rack, A. P. Baddorf, I. N. Ivanov, N. V. Lavrik, F. List, N. Gupta, K. V. Bets, B. I. Yakobson, S. N. Smirnov, *Nat. Mater.* **2018**, 17, 318.
- [13] I. Vlassiouk, P. Fulvio, H. Meyer, N. Lavrik, S. Dai, P. Datskos, S. Smirnov, *Carbon* **2013**, 54, 58.
- [14] Y. Y. Stehle, D. Voylov, I. V. Vlassiouk, M. G. Lassiter, J. Park, J. K. Sharma, A. P. Sokolov, G. Polizos, *Nanotechnology* **2017**, 28, 285601.
- [15] G. Polizos, K. Winter, M. J. Lance, H. M. Meyer, B. L. Armstrong, D. A. Schaeffer, J. T. Simpson, S. R. Hunter, P. G. Datskos, *Appl. Surf. Sci.* **2014**, 292, 563.
- [16] L. H. Karlsson, J. Birch, A. Mockute, A. S. Ingason, H. Q. Ta, M. H. Rummeli, J. Rosen, P. O. A. Persson, *Vacuum* **2017**, 137, 191.
- [17] H. Park, C. Lim, C. J. Lee, J. Kang, J. Kim, M. Choi, H. Park, *Nanotechnology* **2018**, 29, 415303.
- [18] R. Li, Z. Li, E. Pambou, P. Gutfreund, T. A. Waigh, J. R. P. Webster, J. R. Lu, *Langmuir* **2018**, 34, 1827.
- [19] Z. Ni, Y. Wang, T. Yu, Z. Shen, *Nano Res.* **2008**, 1, 273.

- [20] Y. Y Wang, Z. H. Ni, T. Yu, Z. X. Shen, H. M. Wang, Y. H. Wu, W. Chen, A. T. S. Wee, *J. Phys. Chem. C* **2008**, 112, 10637.
- [21] M. M. Lucchese, F. Stavale, E. H. M. Ferreira, C. Vilani, M. V. O. Moutinho, R. B. Capaz, C. A. Achete, A. Jorio, *Carbon* **2010**, 48, 1592.
- [22] R. Beams, L. G. Cancado, L. Novotny, *J. Phys.: Condens. Matter* **2015**, 27, 083002.
- [23] E. H. M. Ferreira, M. V. O. Moutinho, F. Stavale, M. M. Lucchese, R. B. Capaz, C. A. Achete, A. Jorio, *Phys. Rev. B* **2010**, 82, 125429.
- [24] L. G. Cancado, A. Jorio, E. H. M. Ferreira, F. Stavale, C. A. Achete, R. B. Capaz, M. V. O. Moutinho, A. Lombardo, T. S. Kulmala, A. C. Ferrari, *Nano Lett.* **2011**, 11, 3190.
- [25] W. Tian, F. Q. Xie, X. Q. Wu, Z. Z. Yang, *Surf. Interface Anal.* **2009**, 41, 251.
- [26] J. H. Chen, C. Jang, S. Xiao, M. Ishigami, M. S. Fuhrer, *Nat. Nanotechnol.* **2008**, 3, 206.
- [27] K. R. Paton, et al., *Nat. Mater.* **2014**, 13, 624.
- [28] J. H. Park, W. Jung, D. Cho, J. T. Seo, Y. Moon, S. H. Woo, C. Lee, C. Y. Park, J. R. Ahn, *Appl. Phys. Lett.* **2013**, 103, 171609.
- [29] J. Sun, et al., *ACS Nano* **2016**, 10, 11136.
- [30] L. L. Notte, E. Villari, A. L. Palma, A. Sacchetti, M. M. Giangregorio, G. Bruno, A. D. Carlo, G. V. Bianco, A. Reale, *Nanoscale* **2017**, 9, 62.
- [31] J. Lee, D. Berman, *Carbon* **2018**, 126, 225.
- [32] Y. Xu, J. Qu, Y. Shen, W. Feng, *RSC Adv.* **2018**, 8, 15181.

[33] X. Xu, et al., *Adv. Mater.* **2018**, 30, 1702944.

[34] B. Deng, Z. Liu, H. Peng, *Adv. Mater.* **2018**, 1800996

[35] B. Corry, *J. Phys. Chem. B* **2008**, 112, 1427.

[36] B. Mi, *Science* **2014**, 343, 740.

[37] J. Kwak, Y. Jo, S. D. Park, N. Y. Kim, S. Y. Kim, H. J. Shin, Z. Lee, S. Y. Kim, S. Y. Kwon, *Nat. Commun.* **2017**, 8 1549.